The impact of carbon and oxygen abundances on the metal-poor initial mass function

Sharda, P.; Amarsi, A.M.; Grasha, K.; Krumholz, M.R.; Yong, D.; Chiaki, G.; ... ; Nordlander, T.

The impact of carbon and oxygen abundances on the metal-poor initial mass function

Piyush Sharda [1,2,3]★ Anish M. Amarsi [4]★ Kathryn Grasha [1,2]★ Mark R. Krumholz [1,2]
David Yong [1,2] Gen Chiaki [5,6] Arpita Roy [7] and Thomas Nordlander [1,2]

[1]*Research School of Astronomy and Astrophysics, Australian National University, Canberra, ACT 2611, Australia*
[2]*Australian Research Council Centre of Excellence for All Sky Astrophysics in 3 Dimensions (ASTRO 3D), Australia*
[3]*Leiden Observatory, Leiden University, P.O. Box 9513, NL-2300 RA Leiden, The Netherlands*
[4]*Theoretical Astrophysics, Department of Physics and Astronomy, Uppsala University, SE-751 20 Uppsala, Sweden*
[5]*Center for Relativistic Astrophysics, School of Physics, Georgia Institute of Technology, Atlanta, GA 30332, USA*
[6]*Astronomical Institute, Graduate School of Science, Tohoku University, Aoba, Sendai 980-8578, Japan*
[7]*Cosmology Research Group, Scuola Normale Superiore, I-56126 Pisa, Italy*

ABSTRACT

Star formation models predict that the metal-poor initial mass function (IMF) can be substantially different from that observed in the metal-rich Milky Way. This changeover occurs because metal-poor gas clouds cool inefficiently due to their lower abundance of metals and dust. However, predictions for the metal-poor IMF to date rely on assuming solar-scaled abundances, i.e. [X/O] = 0 at all [O/H]. There is now growing evidence that elements such as C and O that dominate metal line cooling in the ISM do not follow solar scaling at low metallicities. In this work, we extend models that predict the variation in the characteristic (or the peak) IMF mass as a function of metallicity using [C/O] ratios derived from observations of metal-poor Galactic stars and of H II regions in dwarf galaxies. These data show [C/O] < 0 at subsolar [O/H], which leads to a substantially different metal-poor IMF in the metallicity range where C I and C II cooling dominate ISM thermodynamics, resulting in an increase in the characteristic mass by a factor as large as 7. An important consequence of this difference is a shift in the location of the transition from a top- to a bottom-heavy IMF upwards by 0.5–1 dex in metallicity. Our findings indicate that the IMF is very sensitive to the assumptions around solar-scaled ISM compositions in metal-poor systems (e.g. dwarf galaxies, the Galactic halo, and metal-poor stars) that are a key focus of *JWST*.

Key words: stars: formation – stars: luminosity function, mass function – ISM: abundances – ISM: clouds – dust, extinction – ISM: general.

1 INTRODUCTION

Understanding the impact of metallicity on the stellar initial mass function (IMF) is of utmost importance for several key areas of galaxy evolution. It is now becoming clear that although the IMF seems to be invariant in the metal-rich components of the Milky Way (Kroupa 2001; Chabrier 2003; Bastian, Covey & Meyer 2010), it could have been different in other environments with metallicities that are subsolar (e.g. Komiya et al. 2007; Mattsson 2010; Suda et al. 2011, 2013; Gennaro et al. 2018; Rossi, Salvadori & Skúladóttir 2021; Filion et al. 2022) or supersolar (e.g. van Dokkum & Conroy 2010; Conroy & van Dokkum 2012; Martín-Navarro et al. 2015; Smith 2020; Gu et al. 2022). It is not surprising that the IMF should be sensitive to the metallicity, since the amount of metals present in the interstellar medium (ISM) directly sets the thermodynamics of the collapsing gas that ultimately forms stars (Omukai 2000; Bromm et al. 2001; Omukai et al. 2005; Omukai, Hosokawa & Yoshida 2010;

Chiaki et al. 2015; Chon, Omukai & Schneider 2021; Sharda & Krumholz 2022).

The number of newly discovered metal-poor stars in the Milky Way and dwarf galaxies has grown exponentially over the past few decades (Frebel & Norris 2015). From a theoretical perspective, several models and simulations have been developed to investigate star formation in low-metallicity environments. However, most of these simulations do not extend down to metallicities low enough ([O/H] < −1.5)[1] that we expect major variations in the IMF (e.g. Myers et al. 2011; Bate 2014; Bate & Keto 2015; Bate 2019).

Only a handful of simulations exist that self-consistently evolve the abundances of different elements in the metal-poor ISM by solving for chemistry on the fly with hydrodynamics (e.g. Chiaki, Yoshida & Hirano 2016; Chon et al. 2021; Chiaki & Yoshida 2022). While these simulations provide a realistic picture of how the abundances of C, N, and O ultimately shape the metal-poor IMF, they cannot disentangle the effects of one element versus another because the evolution of collapsing gas clouds is highly non-linear. Since these

---

★ E-mail: sharda@strw.leidenuniv.nl (PS); anish.amarsi@physics.uu.se (AMA); kathryn.grasha@anu.edu.au (KG)

[1][O/H] = $\log_{10}(O/H) - \log_{10}(O/H)_\odot$.

simulations do not sweep across the possible range of ISM properties and exclude protostellar radiation feedback, they cannot quantify the relative importance of metallicity as compared to physical properties like density and pressure for the IMF (e.g. Munshi et al. 2014; Tanvir, Krumholz & Federrath 2022). This is where analytical models have proved useful owing to the level of control and range one can achieve. Sharda & Krumholz (2022) present an analysis of the thermodynamic budget in collapsing dusty gas clouds across a wide range of metallicities (10^{-6} to 3 times solar) to explore variations in the characteristic mass (or the peak mass, depending on the functional form of the IMF; see section 2.2 of Hopkins 2018) of the IMF. They identify a distinct low-metallicity regime where gaseous metals that are not bound into molecules are the primary contributors to cooling in the ISM, and subsequently set the characteristic mass of the IMF.

However, Sharda & Krumholz (2022) assume solar-scaled abundances to calculate metal line cooling in their models. While this is a reasonable approach to adopt in the first instance, with increasing observational evidence it is becoming clear that several key elements like C and N do not scale with their solar values at low metallicity (see the recent review by Romano 2022). This is because N production changes from primary (not dependent on [O/H]) to secondary (dependent on [O/H]) as the ISM metallicity increases beyond [O/H] > −0.4 (e.g. Edmunds & Pagel 1978; Papadopoulos 2010; Johnson et al. 2022, however, see Roy et al. 2021 for a somewhat more complex picture). Similarly, at low [O/H], C is produced as a primary element; however, its production pathway switches to *pseudo*-secondary at high [O/H] due to enhanced mass loss in the form of stellar winds (e.g. Henry, Edmunds & Köppen 2000; Esteban et al. 2014; Berg et al. 2016). At the lowest metallicities, the individual stellar C, N, and O abundances vary by several orders of magnitude (see fig. 2 of Norris et al. 2013). The primary versus secondary production also impacts the observed metallicity plateau in the gas phase in local galaxies at large galactocentric distances (Grasha et al. 2022), and is important for photoionization modelling of H II regions (Nicholls et al. 2017; Grasha et al. 2021).

The consequence of multiple production pathways is that the [C/O] and [N/O] ratios measured in metal-poor stars in the Galaxy significantly deviate from 0 at low metallicities (Gustafsson et al. 1999; Akerman et al. 2004; Israelian et al. 2004; Spite et al. 2005; Fabbian et al. 2009; Nissen et al. 2014; Amarsi et al. 2019a; Amarsi, Nissen & Skúladóttir 2019c). Similarly, the [C/O] and [N/O] ratios in low-metallicity galaxies also deviate from 0 (Garnett et al. 1995; Kobulnicky & Skillman 1996; Liang et al. 2006; van Zee & Haynes 2006; Pérez-Montero & Contini 2009; Berg et al. 2016, 2019; Nicholls et al. 2017; Roy et al. 2021; Arellano-Córdova et al. 2022). Both these groups of works also find a scatter as high as 0.5 dex in [C/O] at fixed [O/H].

It therefore seems important to take these non-linearities in the [C/O] ratio into account when making predictions for the metal-poor IMF, because C and O are the main metal ISM coolants (Bromm & Loeb 2003; Frebel, Johnson & Bromm 2007). The vast majority of available research in this area has focused on understanding how a non-universal IMF could give rise to the observed trends in [C/O] at low metallicities, but not the other way around (e.g. Garnett et al. 1995; Carigi et al. 2005; Carigi & Hernandez 2008; Mattsson 2010; Tsujimoto & Bekki 2011; Romano et al. 2019a, 2020; Lacchin et al. 2020; Palla et al. 2020). The few works that do look at the influence of C and O cooling on the IMF assume solar-scaled abundances (e.g. Omukai 2000; Chon et al. 2021, 2022) or exclude protostellar radiation feedback (e.g. Schneider et al. 2006; Chiaki & Yoshida 2022). In reality, the IMF and [C/O] ratio influence each other because the IMF sets the yield of C and O from

massive and intermediate-mass stars (e.g. Maeder 1992; Iwamoto et al. 2005; Kobayashi, Karakas & Lugaro 2020), and the ISM C and O abundance directly sets the cooling rate of collapsing molecular gas that dictates the IMF (e.g. Schneider et al. 2012; Chon et al. 2021; Sharda & Krumholz 2022). Additionally, preferential ejection of O through outflows (Mac Low & Ferrara 1999; Chisholm, Tremonti & Leitherer 2018; Sharda et al. 2021a) can also alter the [C/O] ratio in low-metallicity systems (Yin, Matteucci & Vladilo 2011; Berg et al. 2019; Yamaguchi, Furlanetto & Trapp 2022). Thus, it is crucial to understand the dependence of the IMF on the [C/O] ratio in the ISM.

In this work, we extend the calculations of Sharda & Krumholz (2022) by accounting for realistic variations in [C/O] to explore how non-solar-scaled C and O abundances impact the thermodynamics of the metal-poor ISM and thence characteristic stellar mass of the metal-poor IMF. We arrange the rest of the paper as follows: Section 2 summarizes the theoretical framework of Sharda & Krumholz (2022), which we also adopt in this work, Section 3 describes the resulting ISM thermodynamic budget and the IMF when we use a non-zero [C/O], and Section 4 discusses the impact of varying [C/O] as found in observations of metal-poor stars and of H II regions in dwarf galaxies on the characteristic mass of the IMF. Finally, we conclude and provide a future outlook in Section 5.

2 MODEL SUMMARY

The basic premise of the Sharda & Krumholz (2022) model is that radiation feedback from an existing protostar plays a key role in setting the characteristic mass, M_{ch}, of the IMF (Krumholz 2011; Guszejnov, Krumholz & Hopkins 2016; Krumholz et al. 2016). To explore the implications of this *ansatz*, the authors consider a spherically symmetric collapsing dusty gas cloud at a range of densities, pressures, and metallicities. At the centre of this cloud is a protostar, the radiation feedback from which heats the surrounding gas. Following simulations (e.g. Krumholz, Klein & McKee 2011; Federrath & Klessen 2013; Chiaki et al. 2016; Sharda, Krumholz & Federrath 2019; Sharda et al. 2021b) as well as observations (e.g. Caselli & Myers 1995; van der Tak et al. 2000; Schneider et al. 2015; Gieser et al. 2021), the authors adopt a power law for the density profile of the cloud. With such a profile, the dust temperature profile in the presence of radiation feedback is also given by a power law (Chakrabarti & McKee 2005; Krumholz 2011; Chakrabarti et al. 2013). Once the dust temperature is determined, the authors include a variety of thermodynamic processes, such as dust–gas energy exchange, cooling due to metal lines, H_2, HD, cosmic-ray heating, compressional heating, and H_2 formation heating, to find the equilibrium gas temperature. Using the gas temperature profile, the authors then quantify how far away from the existing protostar the cloud becomes Jeans unstable such that it can fragment and collapse to form a new star instead of accreting onto the existing star. The mass that is Jeans unstable is then classified as M_{ch}. We refer the reader to Sharda & Krumholz (2022) for additional information on the model.

Sharda & Krumholz (2022) parametrize metallicity using the generic notation $\mathcal{Z}$ that corresponds to the logarithmic abundance of all metals with respect to solar abundances (Asplund et al. 2009). Since we are interested in studying non-solar-scaled abundances for C and O, we fix our metallicity scale to represent the O abundance (i.e. $\mathcal{Z} \equiv$ [O/H]). We will therefore study how variations in [C/O] as a function of [O/H] impact M_{ch}. The abundances of neutral C and O atoms per H nucleus *in the gas phase* for the solar case that we adopt are $x_{(C, MW)} = 1.4 \times 10^{-4}$ and $x_{(O, MW)} = 3.0 \times 10^{-4}$, following Draine (2011, table 23.1). Our fiducial model uses a solar-scaled

dust-to-gas ratio $\delta = \delta_{MW} \times 10^{[O/H]}$, where $\delta_{MW} = 1/162$ (Zubko, Dwek & Arendt 2004). We also consider an alternative scaling of δ from Rémy-Ruyer et al. (2014) later. We do not differentiate between δ for carbonaceous and silicate grains to calculate the gas–dust energy exchange. This distinction is more important for heating due to H_2 formation on dust (e.g. Cazaux & Spaans 2009) that we do not include in this work. This is because it has a negligible contribution to gas thermodynamics at the location that sets M_{ch} (see section 4.1 of Sharda & Krumholz 2022). We import variations in the chemical state of C and O (C II, C I, O I, and CO) as a function of [O/H] from Sharda & Krumholz (2022, fig. 1), but we also investigate how variations in the chemical state of C and O impact M_{ch} in Section 3.3.

As in Sharda & Krumholz (2022), we study a wide variety of ISM physical conditions by varying the pressure P between $10^4 \, k_B \, \text{K cm}^{-3}$ [representing molecular clouds in main-sequence star-forming galaxies (Dame, Hartmann & Thaddeus 2001; Welty et al. 2016; Miville-Deschênes, Murray & Lee 2017; Kewley et al. 2019)] and $10^8 \, k_B \, \text{K cm}^{-3}$ [representing molecular clouds in starburst galaxies (Turner, Beck & Ho 2000; Bolatto et al. 2008; van Dokkum et al. 2008) or progenitors of superstar clusters and globular clusters (Elmegreen & Efremov 1997; Bastian et al. 2006; Johnson et al. 2015; Finn et al. 2019)]. We also effectively vary the cloud density by sweeping across a range of values for the cloud velocity dispersion σ_v, from 0.5 to 5 km s^{-1} (Padoan, Nordlund & Jones 1997; Myers et al. 2011; Chabrier, Hennebelle & Charlot 2014; Kepley et al. 2016; Sharda et al. 2022). Since the density is given by the ratio of P and σ_v^2, models with low σ_v correspond to the case of high density, and vice-versa. We use density and effective velocity dispersion interchangeably. Thus, our model grid is three-dimensional (3D), sweeping across P, σ_v, and [O/H].

3 RESULTS

3.1 Gas thermal balance

We first discuss how the overall cooling budget of the gas at the location in the cloud where M_{ch} is defined changes when we fix [C/O] to a value other than 0, implying a non-solar scaling of C with respect to O. We remind the reader that M_{ch} is set where the gas mass around an existing protostar in the cloud is sufficient to collapse by itself (i.e. where the enclosed mass equals the Bonnor–Ebert mass; see Ebert 1955; Bonnor 1957). For the purpose of this demonstration, we consider [C/O] = 0 (fiducial model) and [C/O] = −1, and investigate the corners of our grid in P and σ_v. As we will discuss later in Section 4, [C/O] = −1 represents the lowest [C/O] observed in dwarf galaxies (Berg et al. 2019), and a loose lower bound of that measured in metal-poor stars after factoring in uncertainties (Amarsi et al. 2019c).

As in Sharda & Krumholz (2022, equation 31), we quantify the relative contribution of a process η to gas thermodynamics as follows:

$$\mathcal{C}(\eta) = \frac{2\eta}{|\Gamma_c| + |\Gamma_{gd}| + |\Lambda_{gd}| + |\Lambda_M| + |\Lambda_{H_2}| + |\Lambda_{HD}|}, \quad (1)$$

where the Γ terms represent heating processes: Γ_c — compressional heating and Γ_{gd} — heating due to dust–gas energy exchange, and the Λ terms represent cooling processes: Λ_{gd} — cooling due to dust–gas energy exchange, Λ_M — cooling due to fine structure lines of C and O (C I, C II, and O I) as well as cooling due to low-J transitions of CO, Λ_{H_2}— cooling due to lines of H_2 and collisional excitation of H_2, and Λ_{HD} — cooling due to lines of HD and collisional excitation of

HD.[2] When written in this manner, $C(\eta)$ varies from −1 to +1; it is positive if η is a heating process and negative if η is a cooling process. Additionally, absolute values of $C(\eta)$ close to unity imply that the corresponding process η is important for gas thermodynamics. The sum of all heating (cooling) processes is +1 (−1). We also ensure that the luminosity due to all the cooling radiation never exceeds that due to blackbody cooling for all variations of [C/O] we present in this work.

Fig. 1 shows the results for the low-pressure case $P/k_B = 10^4 \, \text{K cm}^{-3}$ with effective velocity dispersion $\sigma_v = 0.5$ (left-hand panel) and 5 km s^{-1} (right-hand panel). We observe cooling due to H_2 and HD dominates at extremely low metallicities ([O/H] $\lesssim$ −5) as expected, and cooling due to dust starts to become significant at high metallicities ([O/H] $\gtrsim$ −2).[3] We also find that cooling due to C and O dominates at intermediate metallicities, as found in Sharda & Krumholz (2022).

We can compare the left- and right-hand panels of Fig. 1 to see the impact of using non-solar-scaled [C/O]. Interestingly, we see that changing the [C/O] ratio has a negligible impact on the gas cooling budget in the model with $\sigma_v = 5$ km s^{-1}. This is because the location of M_{ch} in models with $\sigma_v = 5$ km s^{-1} is much closer to the existing protostar as compared to the models with $\sigma_v = 0.5$ km s^{-1}. Since the gas is denser closer to the protostar, O provides much more cooling as compared to C. However, changing [C/O] to −1 considerably impacts the model with $\sigma_v = 0.5$ km s^{-1} where the location of M_{ch} is farther away from the protostar. Far away from the protostar, the low-density gas is more efficiently cooled by C than O. Thus, the low amount of C as compared to O in the latter case leads to an overall reduction in the cooling provided by metals. As a consequence, the transition where metals start dominating the cooling budget shifts up by more than a dex in metallicity as compared to the model where [C/O] = 0.

Fig. 2 shows the results in the high-pressure case ($P/k_B = 10^8 \, \text{K cm}^{-3}$). In contrast to Fig. 1, we see that there is no appreciable reduction in metal cooling when the abundance of C is reduced by a dex. This is due to O being the primary metal coolant in high-pressure environments, and the fact that dust anyway controls gas thermodynamics at high pressures. Although dust abundance also changes with metallicity, and presumably would change at least somewhat in response to changes in [C/O] (see Section 3.4 for a detailed discussion), at high densities (equivalently, high P) the gas temperature is quite insensitive to the total dust abundance (e.g. Myers et al. 2011; Bate 2019). This is because the dust temperature itself is not altered by the dust abundance as long as there is enough dust to render the circumstellar environment optically thick (true even at very subsolar metallicities due to the high optical/ultraviolet (UV) opacity of dust grains), and because at high densities dust and gas become well-coupled even if the dust abundance is subsolar.

Overall, we learn that a non-solar-scaled [C/O] only impacts the thermodynamics of collapsing dusty molecular clouds at low pressures and low effective velocity dispersions. In this particular case, the transition from an H_2-dominated cooling to metal-dominated cooling occurs at a higher metallicity. The reduced amount of cooling due to a negative [C/O] would lead to higher gas temperatures (since H_2 is a poor gas coolant, e.g. Galli & Palla 1998; Omukai et al. 2005;

[2]As in Sharda & Krumholz (2022), we use the maximum possible cooling due to HD.

[3]Several authors find that dust already becomes a significant gas coolant at [O/H] > −5 (e.g. Schneider et al. 2006; Schneider & Omukai 2010; Meece, Smith & O'Shea 2014; Shima & Hosokawa 2021; Chiaki & Yoshida 2022). The key difference between their work and ours is that we include radiation feedback that heats the dust around the existing protostar.
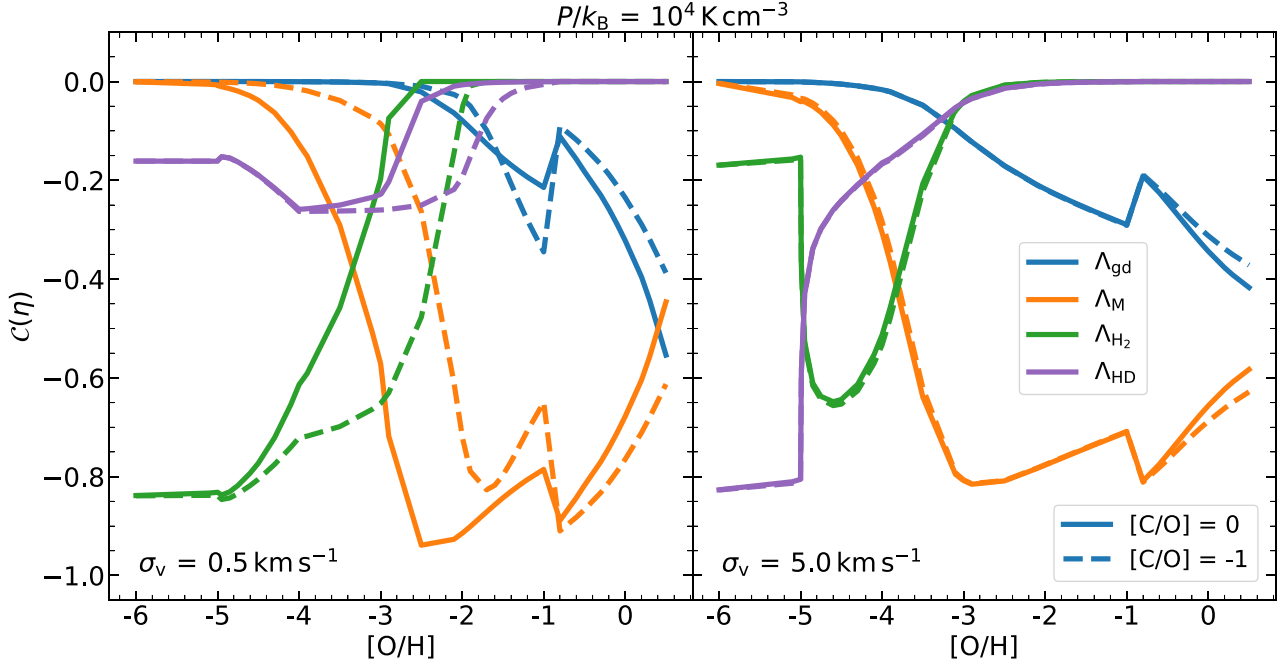
Figure 1. Importance of different cooling processes under thermal balance at the location in the cloud where the characteristic stellar mass of the IMF is defined, $\mathcal{C}(\eta)$, as a function of the oxygen abundance, [O/H]. The results are plotted for pressure $P/k_B = 10^4 \, \mathrm{K \, cm^{-3}}$ and effective velocity dispersion $\sigma_v = 0.5 \, \mathrm{km \, s^{-1}}$ (left-hand panel) and $5 \, \mathrm{km \, s^{-1}}$ (right-hand panel). The solid and dashed curves correspond to models where carbon is solar-scaled ([C/O] = 0) and not solar-scaled ([C/O] = -1), respectively. The cooling processes we study are cooling due to gas–dust energy exchange (Λ_{gd}), metals like C and O (Λ_M), H$_2$ (Λ_{H_2}), and HD (Λ_{HD}). If $\mathcal{C}(\eta)$ is zero for a process η, it is unimportant for cooling the gas. If $\mathcal{C}(\eta)$ is -1, it dominates gas cooling. Non-solar-scaled [C/O] significantly impacts the gas cooling budget for $\sigma_v = 0.5 \, \mathrm{km \, s^{-1}}$ but not for $\sigma_v = 5 \, \mathrm{km \, s^{-1}}$.
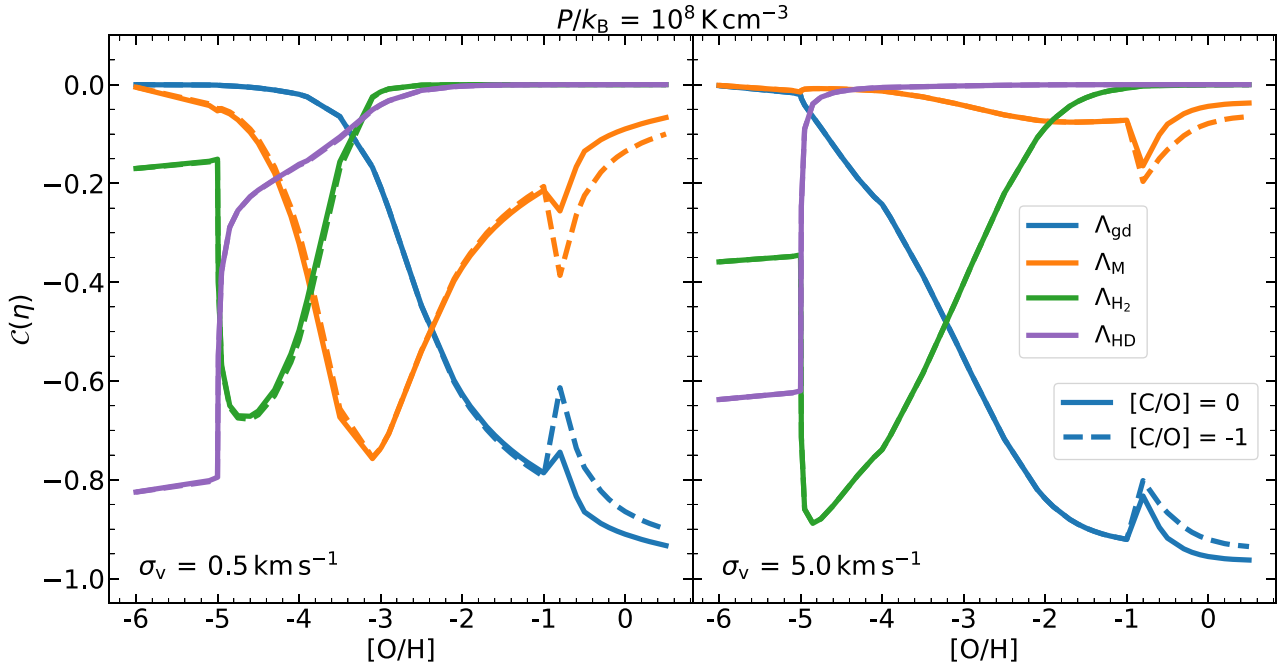
Figure 2. Same as Fig. 1, but for high cloud pressure $P/k_B = 10^8 \, \mathrm{K \, cm^{-3}}$. Non-solar-scaled [C/O] has a negligible impact on the gas cooling budget at high pressure.
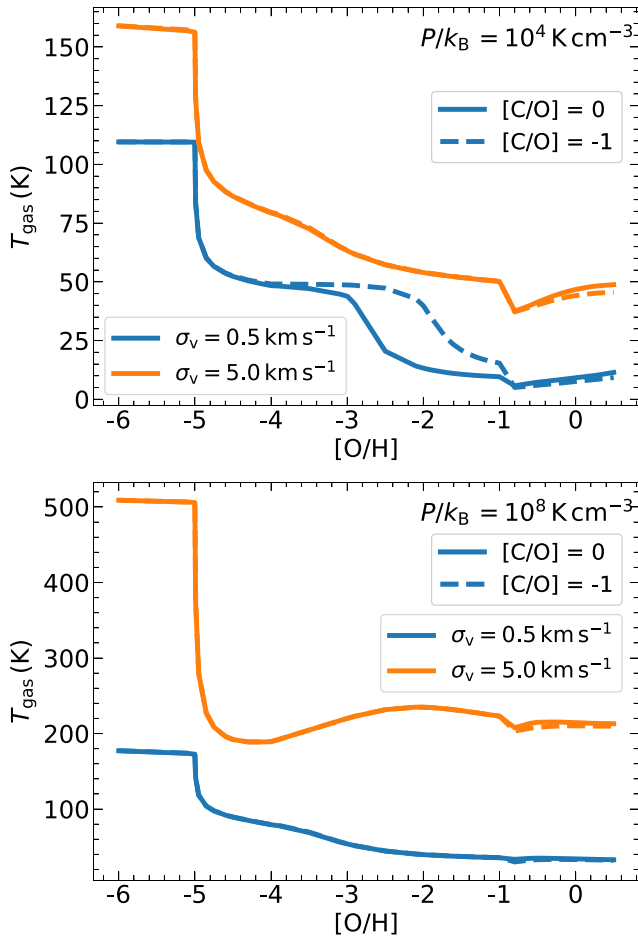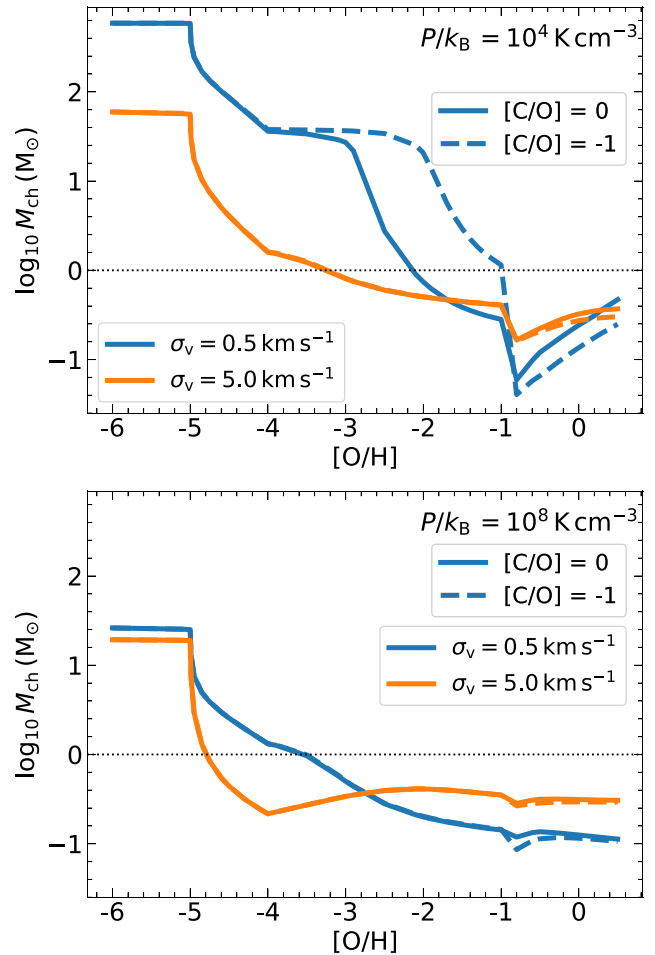
Figure 3. Top panel: Gas temperature, T_{gas}, at the location that sets the characteristic stellar mass as a function of oxygen abundance, [O/H], for a fixed cloud pressure $P/k_B = 10^4 \, K \, cm^{-3}$ at different effective velocity dispersions, $\sigma_v = 0.5 \, km \, s^{-1}$ (blue curves) and $\sigma_v = 5 \, km \, s^{-1}$ (orange curves). The solid and dashed curves correspond to solar-scaled ([C/O] = 0) and non-solar-scaled ([C/O] = −1) carbon abundances, respectively. Bottom panel: Same as the top panel, but for high cloud pressure $P/k_B = 10^8 \, K \, cm^{-3}$. Non-solar-scaled [C/O] changes the gas temperature as $-4 \leq$ [O/H] ≤ -1 at low P and low σ_v.

Figure 4. Top panel: Characteristic stellar mass, M_{ch}, as a function of oxygen abundance, [O/H], for a fixed cloud pressure $P/k_B = 10^4 \, K \, cm^{-3}$ at different effective velocity dispersions, σ_v, as shown in the legend. The solid and dashed curves correspond to solar-scaled ([C/O] = 0) and non-solar-scaled ([C/O] = −1) carbon abundances, respectively. M_{ch} increases by a factor as high as 7 at $-4 \leq$ [O/H] ≤ -1 when [C/O] = −1. Bottom panel: Same as the top panel, but for high cloud pressure $P/k_B = 10^8 \, K \, cm^{-3}$. M_{ch} is not impacted by non-solar-scaled [C/O] at high P.

Glover & Clark 2012), which is what we see from the top panel of Fig. 3. Since a negative [C/O] does not impact the gas thermal balance in high-pressure environments, the gas temperature does not deviate from the model with [C/O] = 0 (see the bottom panel of Fig. 3).

3.2 Characteristic stellar mass of the IMF

We characterize the IMF as bottom-heavy if the characteristic stellar mass $M_{ch} < 1 \, M_\odot$, and top-heavy otherwise. The variations in the gas temperatures affected by reducing [C/O] discussed in Section 3.1 directly impact M_{ch} because the temperature structure of the gas determines the Bonnor–Ebert mass.

We see from Fig. 4 that the high-σ_v or high-P models, for which the gas temperature is insensitive to changes in [C/O], also do not show any variations in M_{ch} as a function of [O/H]. However, M_{ch} significantly changes for the model with low σ_v and low P, where metal cooling is dominated by C. The higher gas temperatures due

to the lower amount of C in the case with [C/O] = −1 result in higher M_{ch} because the location where the enclosed mass equals the Bonnor–Ebert mass shifts further away from the existing protostar in the cloud. For example, M_{ch} increases from ∼3 to 34 $M_\odot$ around [O/H] = −2.5. Additionally, the transition where the IMF is expected to become bottom-heavy now occurs around [O/H] ∼ −1 instead of [O/H] ∼ −2 as in the fiducial model with [C/O] = 0. Thus, a non-zero [C/O] matters for M_{ch} (and consequently, for the IMF) at low pressures and high densities.

Using [C/O] = −1 at [O/H] > −1 also has a minor but noticeable effect on M_{ch}. In this case, we observe from Fig. 4 that [C/O] = −1 produces a lower M_{ch} as compared to the fiducial model with [C/O] = 0. This is opposite of the influence of a lower [C/O] at [O/H] < −1, and occurs because of enhanced CO cooling due to higher gas density as the equilibrium location where the enclosed mass equals the Bonnor–Ebert mass shifts further away from the existing protostar. Nonetheless, this effect is likely not realistic since we expect [C/O] to be closer to zero near [O/H] ∼ 0.
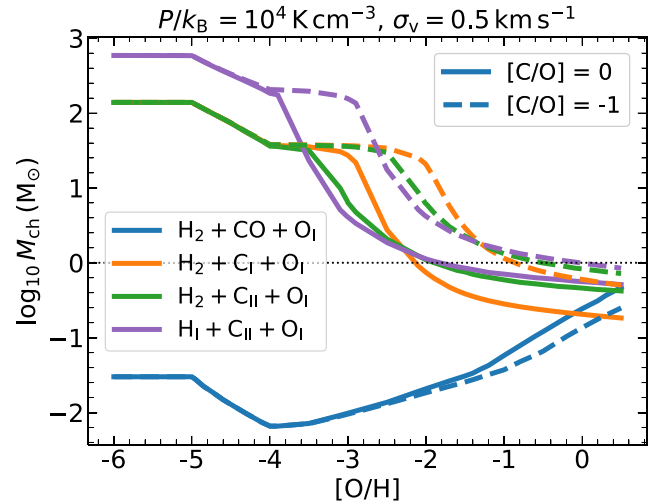
3.3 Effects of different chemical states of C and O

So far, we have assumed a particular chemical state of C and O as a function of [O/H] (fig. 1 Sharda & Krumholz 2022). Specifically, we have assumed that most C atoms are in the form of C^+ at primordial-like [O/H], C at intermediate [O/H], and CO at high [O/H]. Similarly, for O, we have assumed that most of the O atoms exist in the form of neutral O in the low-[O/H] ISM; however, roughly half of them are locked in CO at high [O/H]. While there are sound theoretical arguments (e.g. Omukai et al. 2005; Krumholz, McKee & Tumlinson 2009; McKee & Krumholz 2010; Glover & Clark 2012, 2016; Sternberg et al. 2014; Bialy & Sternberg 2015; Chiaki et al. 2015; Hu, Sternberg & van Dishoeck 2021; Sternberg, Gurman & Bialy 2021; Chiaki & Yoshida 2022) as well as some observational support (Langer 2009; Rubio et al. 2015; Shi et al. 2016; Pineda et al. 2017; Schruba et al. 2017; Jameson et al. 2018; Madden et al. 2020; Guadarrama et al. 2022) for our choice of C and O chemical states at different [O/H], it only statistically represents reality, and we expect considerable scatter or co-existence of different chemical states in individual low-metallicity ISM environments.

Noteworthy in this context are the suite of simulations at very low metallicities (ranging $-6 \leq$ [O/H] ≤ -3) carried out by Chiaki et al. (2016), Chiaki & Wise (2019), and Chiaki & Yoshida (2022). The authors start by assuming that the low-metallicity ISM is enriched by a Population III supernova, which sets the initial abundances of the different elements and their chemical states. The authors follow the evolution of various chemical states of C and O, and find that carbon mostly exists as C or C^+ at densities less than $10^4 - 10^5 \, cm^{-3}$, beyond which it is locked in CO, irrespective of [O/H]. Similarly, regardless of [O/H], O is mostly present in the neutral form at densities less than $10^4 \, cm^{-3}$, OH and O_2 at densities around $10^4 - 10^8 \, cm^{-3}$, and H_2O at higher densities. In principle, we can adopt their results to construct the chemical makeup of C and O in our models as a function of the density. However, these authors do not consider dissociation of molecules from UV photons emitted by background stars or stars within the same cloud. One-zone calculations by Omukai (2012) that include this far-ultraviolet (FUV) feedback at [O/H] < -3 find that even a weak FUV field can significantly impact the chemical composition and subsequent thermal evolution of the clouds at densities lower than $10^8 \, cm^{-3}$. Since the densities at which we calculate M_{ch} are typically in the range of $10^3 - 10^7 \, cm^{-3}$, this implies that the chemical composition of C and O as presented in the above simulations is very sensitive to FUV feedback.

As a simpler alternative, we create a grid of models with four distinct chemical compositions: (1) H_2 + CO + O I, (2) H_2 + C I + O I, (3) H_2 + C II + O I, and (4) H I + C II + O I for all [O/H]. The first composition is such that all C is locked in CO, and the remaining O atoms not locked in CO exist as O I. Note that not all of these combinations are realistic, at least not for all [O/H]. We deliberately sweep across a larger-than-reasonable parameter space to explore possible variations in M_{ch} at non-zero [C/O] for different chemical states.

In the previous sections, we have demonstrated that the effects of a non-zero [C/O] for different chemical compositions are only significant for the case where the pressure and velocity dispersion are low. Therefore, we only present results for this case in Fig. 5. The trends we find corroborate our findings above. The case where the gas is almost fully molecular (H_2 + CO + O I) exhibits a bottom-heavy IMF even at very low [O/H]. This is because low-J lines of CO provide more cooling than the fine structure lines of C I, C II, and O I for the densities we are concerned with, and the CO cooling

Figure 5. Same as Fig. 4 but for different chemical states across [O/H] (as shown in the legend) for a fixed pressure $P/k_B = 10^4 \, K \, cm^{-3}$ and effective velocity dispersion $\sigma_v = 0.5 \, km \, s^{-1}$. Variations in M_{ch} for non-solar-scaled [C/O] are robust to *realistic* chemical states of C and O at [O/H] < -1 (orange, green, and purple curves).

rate is largely insensitive to the CO abundance. Since the low-J lines of CO are very optically thick, so a reduction in CO abundance is compensated by a reduction in optical depth, leaving the net cooling rate almost unchanged (van der Tak et al. 2007; Krumholz 2014). However, as we discuss above, this case is not realistic, since we do not expect a CO-dominated chemical state at low C and O abundance for the densities we are concerned with.

We see that for the other two models where hydrogen is molecular (orange and green curves), the transition from a top- to bottom-heavy IMF occurs at higher [O/H] when [C/O] $= -1$, compared to when [C/O] $= 0$. Moreover, for all the models where CO is absent (orange, green, and purple curves, all having different chemical states of H and C), the resulting M_{ch} increases by a factor ~ 2 at [O/H] $= 0$ when [C/O] $= -1$, compared to when [C/O] $= 0$. While the resulting M_{ch} is not realistic since we know C and O primarily exist in the form of CO at high [O/H], it shows the impacts a non-zero [C/O] can have based on the chemical state of C and O.

To summarize, we find that the trends in M_{ch} for non-zero [C/O] are robust to variations in the chemical state of C and O. However, the exact [O/H] where the transition from a top- to bottom-heavy IMF occurs is sensitive to the chemical makeup of C and O in the gas.

3.4 Effects of a varying dust-to-metal ratio

It has been long known that there is a correlation between the ISM gas-phase C abundance and the dust-to-gas ratio (Cohen et al. 1989; Mathis 1990). The amount of C available in the gas phase depends on the fraction of C locked in dust grains, which is different at different metallicities (e.g. Konstantopoulou et al. 2022). Thus, the dust-to-metal ratio can play a role in setting M_{ch}. So far, we have used a simple scaling of the dust-to-metal ratio, $\delta \propto$ [O/H]. It is therefore worth analysing how our results change if we use a different scaling of the dust-to-metal ratio with [O/H]. For this purpose, following Rémy-Ruyer et al. (2014), we set $\delta \propto 10^{[O/H]}$ for [O/H] ≥ -0.7, and $\delta \propto 10^{3.1[O/H]}$ for lower [O/H].

Fig. 6 plots the trends in M_{ch} at low pressure and high density (or low effective velocity dispersion) for the modified scaling of dust-
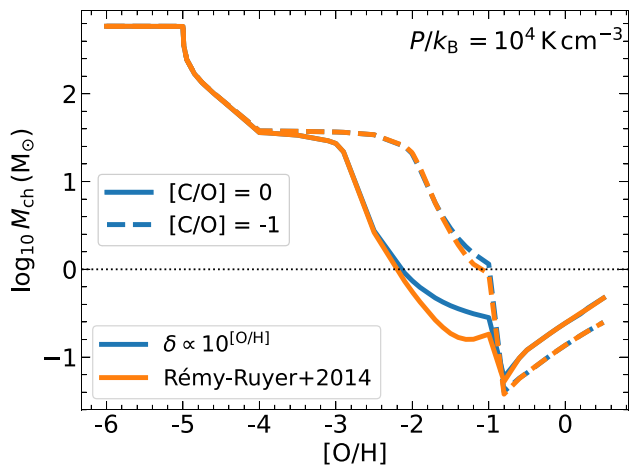
Figure 6. Blue curves are the same as Fig. 4 for pressure $P/k_B = 10^4$ K cm^{-3} and effective velocity dispersion $\sigma_v = 0.5$ km s^{-1}, using a linear scaling of the dust-to-metal ratio δ with [O/H]. Orange curves are for models using the dust-to-metal ratio scaling with [O/H] from Rémy-Ruyer et al. (2014). The Rémy-Ruyer et al. (2014) scaling of δ with [O/H] makes little difference to the resulting trends in M_{ch}.

to-metal ratio with [O/H], for the two cases where [C/O] $= 0$ and [C/O] $= -1$. While a different dust-to-metal ratio scaling produces slightly different trends in M_{ch} due to Γ_{gd} and Λ_{gd}, the variations in M_{ch} due to a non-zero [C/O] are similar to those we have noticed in Sections 3.2 and 3.3. We also find that the trends in M_{ch} at high pressure for a non-zero [C/O] do not vary if we change the scaling of the dust-to-metal ratio with [O/H].

Note that there are several other models/simulations that describe the evolution of δ with [O/H] (Popping, Somerville & Galametz 2017; Hou et al. 2019; Li, Narayanan & Davé 2019; Vijayan et al. 2019; Triani et al. 2020). However, none of them seem to reproduce the observed data across a wide range of metallicities and redshifts (see the discussion in Popping & Péroux 2022). We therefore do not attempt to test variations in M_{ch} due to the $\delta - $[O/H] relations predicted by these models, but note that this is an important avenue with significant potential for future exploration.

4 IMPACT OF VARIATION IN [C/O] ON THE METAL-POOR IMF

Having obtained a basic intuition of variations in M_{ch} as a function of [C/O], we now turn to available measurements of [C/O] at different [O/H], and use these data to systematically predict variations in M_{ch}. We focus on two sets of data: one from high-resolution spectroscopic observations of metal-poor stars in the Milky Way, and other from gas-phase abundance measurements in H II regions of metal-poor dwarf galaxies.

4.1 Insights from observations of metal-poor stars

The last decade has seen an immense progress in abundance measurements of metal-poor stars in the Milky Way (Norris et al. 2013; Arentsen et al. 2020; Youakim et al. 2020; Yong et al. 2021; Lucey et al. 2022) as well as in dwarf galaxies (e.g. Frebel et al. 2010, 2016; Ishigaki et al. 2014; Ji et al. 2016; Abohalima & Frebel 2018; Chiti et al. 2018; Nagasawa et al. 2018; Aoki, Aoki & François 2020). The abundance patterns observed in metal-poor stars carry signatures of the primordial (or primordial-like) ISM they were

born in, and thus provide much needed observational constraints on the metal-poor ISM (e.g. Caffau et al. 2011; Johnson 2015; Ezzeddine et al. 2019; Frebel et al. 2019; Nordlander et al. 2019; Skúladóttir et al. 2021; Mardini et al. 2022). Carbon, in particular, has received special emphasis in these studies because early results discovered high [C/Fe] in stars with [Fe/H] < -2, now known as carbon-enhanced metal-poor stars (CEMP, Beers & Christlieb 2005; Frebel & Norris 2015), with [C/Fe] $> +0.7$ (Aoki et al. 2007).[4] While there are still discrepancies that exist between measurements from different surveys (Arentsen et al. 2022), the general consensus is that the evolution of C is highly non-linear in metal-poor environments. Thus, the measured trends in [C/O] in metal-poor stars are promising as a diagnostic of the metal-poor IMF.

Direct measurements of O in metal-poor stars are challenging as the atomic lines in the optical become vanishingly weak at [O/H] < -2; at such low metallicities only the near-UV molecular OH lines can be used, which requires significant investment in time on large telescopes with highly efficient UV spectrographs (Bessell, Hughes & Cottrell 1984; Bessell, Sutherland & Ruan 1991; Boesgaard et al. 2011). Moreover, molecular lines are expected to be strongly susceptible to assumptions about the model atmosphere at low metallicity (Collet, Asplund & Trampedach 2006, 2007; García Pérez et al. 2006; Frebel et al. 2008; González Hernández et al. 2010; Gallagher et al. 2016, 2017; Norris & Yong 2019). Thus, measured [C/O] ratios in these stars are hard to come by. Moreover, the abundances, if measured using approximate 1D or local thermodynamic equilibrium stellar atmosphere models (e.g. Norris et al. 2013; Nissen et al. 2014), need complex corrections (e.g. Amarsi et al. 2016; Nissen & Gustafsson 2018). In fact, C abundances are severely impacted by 3D non-local thermodynamic equilibrium (3D-NLTE) corrections, which have led to several CEMP stars being re-classified as C-normal stars (Norris & Yong 2019; Amarsi et al. 2019a).

To avoid these caveats, we use the C and O abundances presented by Amarsi et al. (2019c) for a sample of 187 FG-type main-sequence stars in the Galactic thin and thick discs as well as in the metal-poor halo. The abundances were inferred via a re-analysis of the data presented in Nissen et al. (2007, 2014), by using 3D radiative-hydrodynamic stellar atmosphere models from the Stagger-grid (Collet, Magic & Asplund 2011; Magic et al. 2013) combined with 3D radiative transfer taking NLTE effects into account. The C and O abundances are based on C I and O I lines of high excitation potential (Amarsi et al. 2018, 2019b). The advantage of this is that they have similar sensitivities to stellar parameters, and so uncertainties in the measured stellar effective temperature and surface gravity should cancel out to first order in the [C/O] ratio (Amarsi et al. 2019a).

The top panel of Fig. 7 shows the trends in [C/O] as a function of [O/H] in the observed sample.[5] We fit the observed trend with a

---

[4]What matters for gas cooling by metals in the ISM is the [C/O] ratio, and not the [C/Fe] or [O/Fe] ratios, since the abundance of Fe in the gas phase is tiny. Thus, for the purpose of our work, a high [C/Fe] or [O/Fe] has similar implications on the IMF as Sharda & Krumholz (2022) if [C/O] $= 0$.

[5]The [C/H] and [O/H] measured by Amarsi et al. (2019c) are normalized via a similar analysis for the Sun as for their stars, corresponding to solar carbon and oxygen abundances of $12 + \log_{10}$ C/H $= 8.43$ and $12 + \log_{10}$ O/H $= 8.68$, respectively. The reader might notice that the solar abundance for C and O atoms per H nucleus we use ($x_{C, MW} = 1.4 \times 10^{-4}$ and $x_{O, MW} = 3 \times 10^{-4}$) for the models is lower than the earlier values by $\sim$40 per cent. The reason for this discrepancy is that a fraction of the C and O atoms in the ISM are locked in dust grains (e.g. SiO, FeO, etc.). This difference does not matter for this work since we normalize the model results by the gas-phase solar O
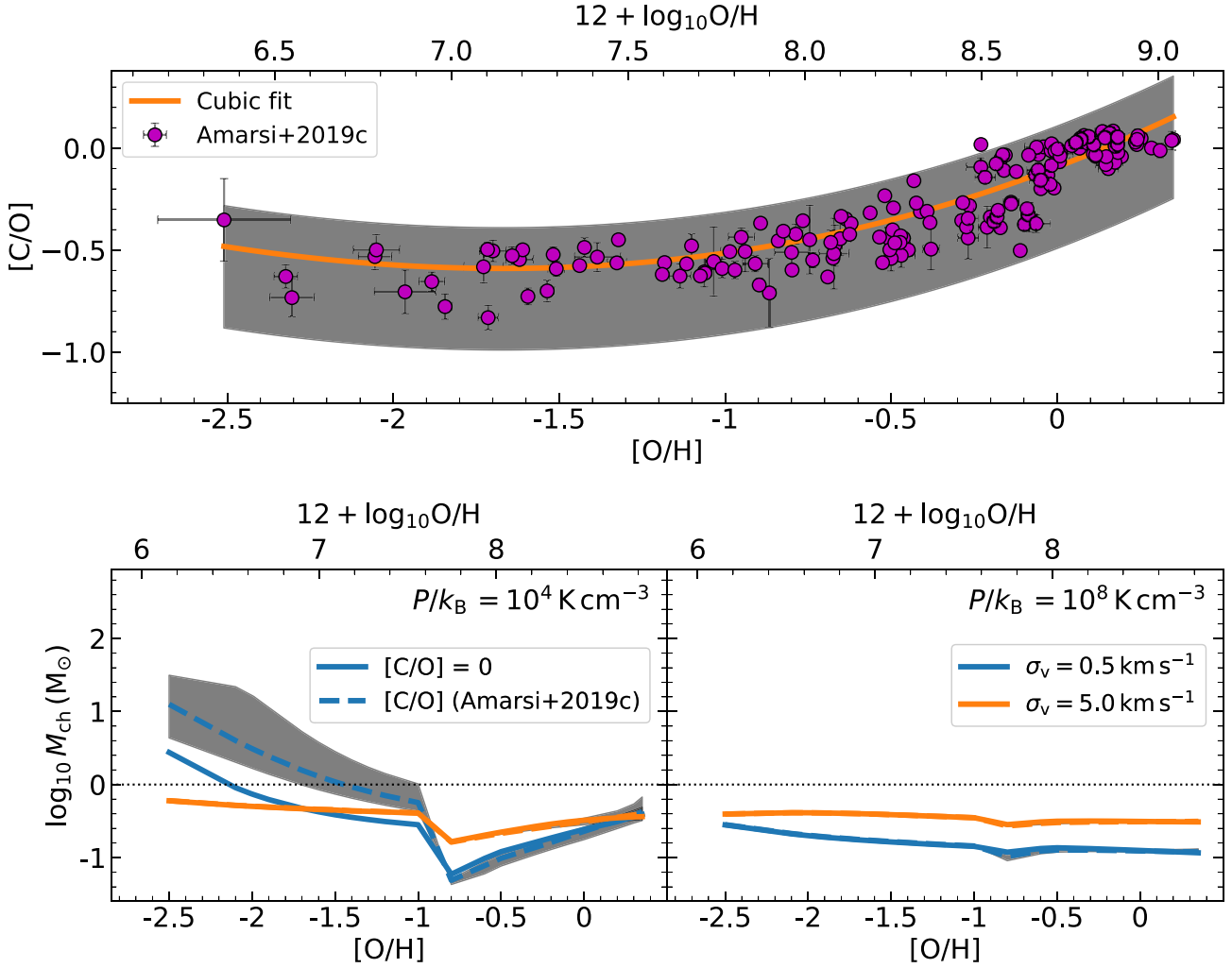
Figure 7. Top panel: Observed trends in [C/O] as a function of [O/H] from 3D-NLTE abundance modelling of metal-poor Milky Way stars (Amarsi et al. 2019c). The orange curve represents a cubic polynomial fit to the data, and the grey-shaded region encompasses [C/O] higher (lower) than the best-fitting by 0.2 (0.4) dex. Bottom panel: Trends in the characteristic IMF mass, M_{ch}, as a function of [O/H] from the models. The solid curves represent the models from Sharda & Krumholz (2022) that use [C/O] = 0. The dashed curves represent models where [C/O] varies with [O/H] following the cubic fit to the data plotted in the top panel. The grey-shaded region corresponds to M_{ch} values when [C/O] is higher (lower) than the best-fitting by 0.2 (0.4) dex. The conversion from [O/H] to $12 + \log_{10}$ O/H is different by 0.22 dex between the top and bottom panels due to different normalizations for solar O abundance in stars versus in the gas phase because of depletion in the latter.

simple cubic polynomial (orange curve) weighted by the measured 1σ uncertainty in [C/O]:

$$[C/O] = a_C[O/H]^3 + b_C[O/H]^2 + c_C[O/H] + d_C, \quad (2)$$

where the best-fitting $a_C = -0.02$, $b_C = 0.14$, $c_C = 0.60$, and $d_C = -0.09$. To cover the scatter present in the data, we simply increase (decrease) the best-fitting [C/O] by +0.2 (−0.4) dex. We notice that the mean [C/O] ∝ [O/H] at [O/H] > −1; however, it remains roughly constant for $-2 \leq [O/H] \leq -1$ (see also Romano et al. 2019a, 2020). Below [O/H] = −2, the data are too scarce to draw any meaningful conclusions, although the cubic polynomial fit shows an upturn in [C/O] at the lowest [O/H] due to the most metal-poor star. This upturn has also been noticed in other works; e.g. in damped Ly α

abundance, and the data by the O abundance measured in the Sun assuming no depletion. We refer the reader to Draine (2011) for a detailed discussion of C and O abundances in different components of the Galaxy.

absorbers (Akerman et al. 2005; Cooke, Pettini & Jorgenson 2015; Cooke, Pettini & Steidel 2017) as well as EAGLE cosmological simulations (Sharma et al. 2018). Some authors attribute it to enrichment from Population III supernovae (Fabbian et al. 2009; Salvadori & Ferrara 2012), while others argue for enrichment from low-metallicity asymptotic giant branch (AGB) stars (Sharma et al. 2018). If this upturn were real, it would imply that [C/O] tends to approach zero again at low [O/H], so the resulting M_{ch} at low [O/H] would be similar to that reported in Sharda & Krumholz (2022); e.g. $M_{ch} \approx 20\,M_\odot$ at [O/H] = −3.

Before we present the results from the model, a key question to address here is whether the [C/O] ratios that Amarsi et al. (2019c) find are representative of the [C/O] ratio of the ISM out of which these stars formed (e.g. Bonifacio et al. 2015), because our IMF models use ISM abundances. Given that all the stars in this sample are C-normal ([C/Fe] < +0.7; see Amarsi et al. 2019c, fig. 11), it is not likely that C was accreted later on due to mass transfer by a companion (as is the case for s process-rich CEMP-s stars; see

Abate et al. 2015 and Arentsen et al. 2019). Moreover, these main-sequence stars have not undergone any helium burning, precluding any intrinsic enhancement of C on the stellar surface. Thus, we can safely assume that the C abundances measured in these stars reflect the intrinsic ISM C abundance out of which they were born. Another category of CEMP stars is called CEMP-no, which do not show an enhancement in *s*-process elements (e.g. Yoon et al. 2016; Arentsen et al. 2019). A fraction of these stars is proposed to have evolved in isolation (Yoon et al. 2019), so their [C/O] ratios should also reflect the ISM [C/O] that they were born with (Bonifacio et al. 2015; Hansen et al. 2016; Norris & Yong 2019; Lucey et al. 2022; Zepeda et al. 2022). While the available O measurements in CEMP-no stars suggest [C/O] ~ 0 (fig. 8, Frebel & Norris 2015), the scatter is quite large, and for a large fraction of stars only O abundance limits are available due to the reasons we mention above. Future observations that focus on obtaining O abundances in CEMP-no stars is therefore crucial to constraining their IMF.[6]

Using the best-fitting [C/O]–[O/H] relation, we produce the trends in M_{ch}–[O/H] at low and high pressures. The bottom panels of Fig. 7 show the results. Not surprisingly, the trends in M_{ch} at high pressure remain unaffected due to varying [C/O] as suggested by the data. The only appreciable difference in M_{ch} for a varying [C/O] occurs in models with low pressure and high density (blue curves in the bottom-left panel). At low metallicity ([O/H] < -1), as compared to the fiducial model with [C/O] $= 0$, we find that a varying [C/O] produces M_{ch} higher by a factor $\lesssim 5$. Additionally, the metallicity ([O/H]) where the IMF transitions from top- to bottom-heavy shifts by somewhere between $+0.4$ and $+1.1$ dex; the exact location of the transition is uncertain owing to the scatter present in the data, which corresponds to the grey-shaded region around the dashed blue curve in the bottom panel of Fig. 7. Interestingly, at high metallicity ([O/H] > -1), we also find that the scatter in the data introduces uncertainty in M_{ch} by a factor $\lesssim 2$. While a factor of 2 variation in M_{ch} is not substantial when M_{ch} is large, it can have measurable consequences when M_{ch} is subsolar, because subsolar stars live for much longer.

Overall, the non-constant [C/O] as measured in metal-poor stars would have influenced the IMF for the next generation of stars in a low-pressure and high-density ISM. Additionally, in such an environment, the data suggest that the transition to a bottom-heavy IMF would occur later on, after the ISM was enriched to 1 dex higher in O. However, a non-constant [C/O] would have had no significant impact on the characteristic stellar mass if the ISM was highly pressurized.

4.2 Insights from observations of metal-poor dwarf galaxies

Metal-poor dwarf galaxies are ideal laboratories to test variations in the IMF since the physical conditions therein are quite different from those in the Milky Way (e.g. Gennaro et al. 2018). The abundances of nebular C and O have been measured in several metal-poor dwarf galaxies using high-resolution UV spectroscopy (Garnett et al. 1995, 1999; Berg et al. 2016, 2019; Llerena et al. 2022). The collisionally excited UV lines of C III and O III that are used to measure the [C/O] ratio do not suffer from reddening since the interstellar extinction is invariant over 1600–2000 Å (Byler et al. 2018; Mingozzi et al.

2022). These lines are also largely insensitive to variations in the physical conditions of the H II regions. Additional measurements have also been obtained using the optical recombination lines of C II and O II (López-Sánchez et al. 2007; Esteban et al. 2009, 2014). The resulting trends from the optical data are similar to that obtained from UV lines (e.g. Esteban et al. 2014; Toribio San Cipriano et al. 2017); however, the abundances can differ by as high as 0.3 dex (the so-called abundance discrepancy problem, see García-Rojas & Esteban 2007; López-Sánchez et al. 2007). Additional uncertainty can arise from ionization correction factors that are applied to take into account the existence of other ionized states of C and O which are not directly measured (Stasińska 1978; Garnett et al. 1999; Esteban et al. 2014; Berg et al. 2016).

The top panel of Fig. 8 shows measurements of the [C/O] ratio as a function of [O/H] in 93 metal-poor dwarf galaxies that we adopt from Berg et al. (2019), which includes data compiled from various studies, including at redshifts (*z*) 2–3 (Pilyugin & Thuan 2005; García-Rojas & Esteban 2007; López-Sánchez et al. 2007; Esteban et al. 2009, 2014; Erb et al. 2010; Christensen et al. 2012; Bayliss et al. 2014; James et al. 2014; Stark et al. 2014; Steidel et al. 2016; Vanzella et al. 2016; Amorín et al. 2017; Berg et al. 2018; Rigby et al. 2018)[7]. Note that these data are not corrected for the depletion of C and O onto dust, largely due to uncertainties in the chemical evolution of C in the diffuse and the ionized ISM at low metallicities (Draine 2011; Sofia et al. 2011; Jenkins 2014). Some authors argue for a correction factor due to dust depletion of ~ 0.1 dex for both C and O at high metallicities (Peimbert & Peimbert 2010; Esteban et al. 2014), which would leave the [C/O] ratio invariant to dust depletion. However, this effect is proposed to be smaller at low metallicities due to small extinctions (Berg et al. 2019).

In the top panel of Fig. 8, we also overplot the empirical relation developed by Nicholls et al. (2017) based on scaling relations using stellar and gas-phase abundances data:

$$[C/O] = \log_{10}\left[10^{e_C} + 10^{\log_{10}(O/H)+f_C}\right] , \tag{3}$$

where $e_C = -0.8$ and $f_C = 2.72$. The data show a trend where [C/O] is roughly constant for [O/H] < -0.7, and linearly increases with [O/H] otherwise (Nicholls et al. 2017). However, given the uncertainty and the scatter in the measurements, the trend can be equally well described by a monotonically increasing function in [O/H] (Garnett et al. 1995). The former has been interpreted to reflect the primary production of C at low [O/H] from intermediate-mass stars, and a pseudo-secondary production at high [O/H], possibly from winds of $M_\star > 10 \, M_\odot$ stars, while the latter reflects the possibility of pseudo-secondary C production down to the lowest measured [O/H]. Nonetheless, it is clear that the average [C/O] < 0 for the range of [O/H] covered by the data. A negative [C/O] could also be shaped by dwarf galaxies preferentially losing oxygen in galactic outflows, as predicted by both the theory of ISM metallicity (Mac Low & Ferrara 1999; Dalcanton 2007; Robles-Valdez et al. 2017; Emerick et al. 2018; Romano et al. 2019b; Sharda et al. 2021a, c) and observations of galactic outflows in dwarf galaxies (Chisholm et al. 2018; Lopez et al. 2020; Cameron et al. 2021).

We use the empirical relation of Nicholls et al. (2017) to predict variations in M_{ch} for the four canonical models with low/high pressures and effective velocity dispersions (or densities). To encapsulate the scatter present in the data, we simply change the resulting [C/O]

---

[6]In the absence of O measurements, Mg is often used as a tracer for oxygen (or, more broadly speaking, for α elements). However, at low [O/H], available data suggest that Mg does not trace O very well. In fact, there is considerable discrepancy in [O/Mg] at low [O/H] within different Galactic surveys (Buder et al. 2021; Abdurro'uf et al. 2022; Hayes et al. 2022).

[7]Similar to the stellar data we use in Section 4.1, the Berg et al. (2019) data are normalized to a solar C abundance of $12 + \log_{10} C/H = 8.43$ and solar O abundance of $12 + \log_{10} O/H = 8.69$ (Grevesse et al. 2010).
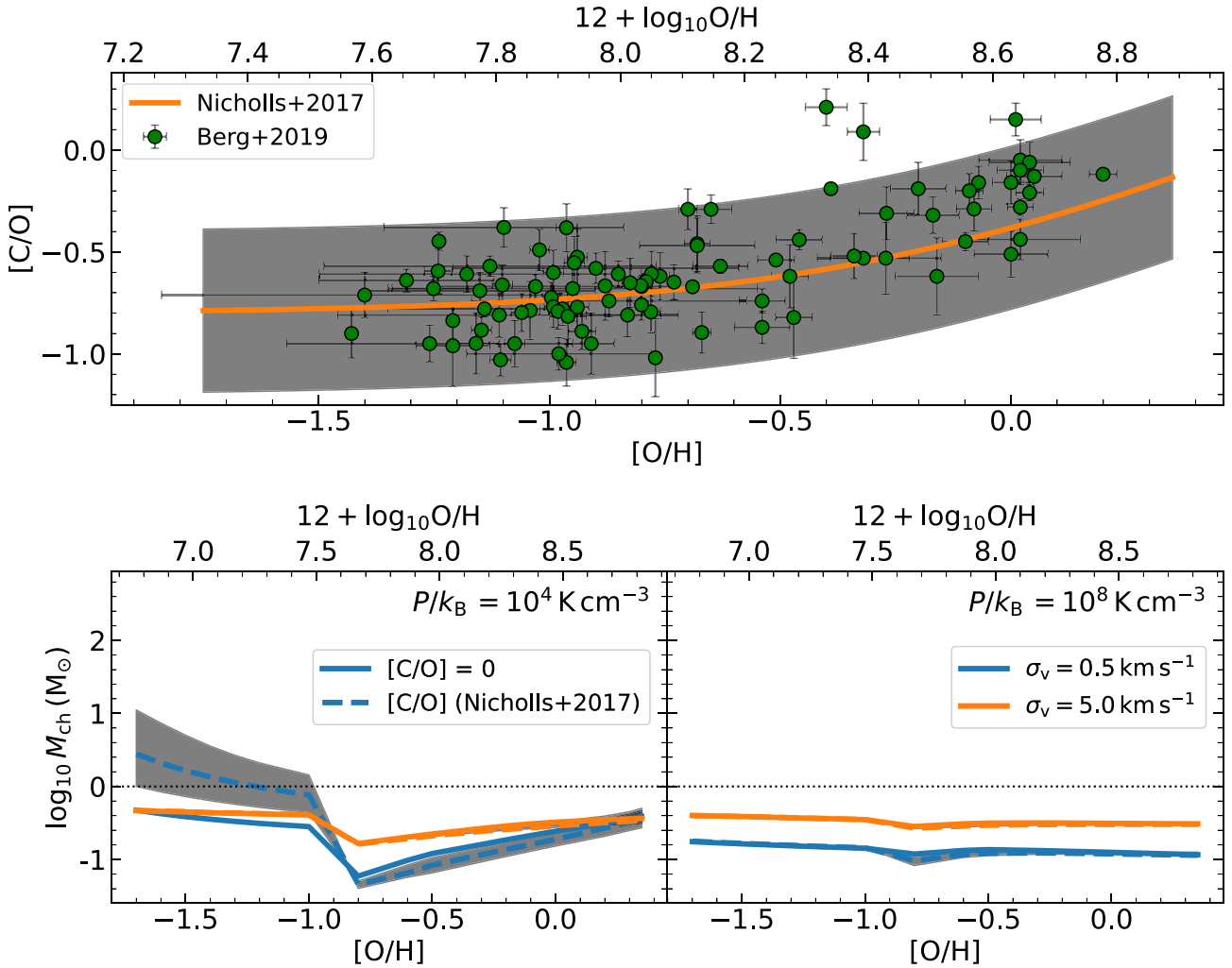
Figure 8. Same as Fig. 7 but for gas-phase (ISM) measurements from H II regions in metal-poor dwarf galaxies. The data plotted in the top panel are taken from Berg et al. (2019). The orange curve in the top panel represents the empirical [C/O]–[O/H] relation from Nicholls et al. (2017). The grey-shaded region encompasses [C/O] different than the best-fitting by ± 0.4 dex.

by ± 0.4 dex at all [O/H], as shown with the grey-shaded region in the top panel of Fig. 8. The bottom panel of Fig. 8 presents the results, which are qualitatively similar to what we find in Section 4.1 (Fig. 7) from observations of metal-poor stars. As in Section 3, we see that a varying [C/O] only impacts the model with low pressure and high density (blue curves in the bottom-left panel). The consequence of a varying [C/O] ratio according to the Nicholls et al. relation is that $M_{\rm ch}$ can be larger by a factor $\lesssim 7$ compared to the default case where C and O scale together. Additionally, we also see that the IMF does not transition to bottom-heavy until the gas-phase oxygen abundance exceeds 7.5 on the absolute scale (or [O/H] > −1.2). This is considerably different from the case where C and O scale together, and the IMF transitions to bottom-heavy at an oxygen abundance that is smaller by an order of magnitude. This is further complicated by the scatter present in the data, as the grey-shaded band in the bottom panel of Fig. 8. The impact of the observed trends in [C/O] as a function of [O/H] remains negligible at high pressures.

Thus, we find that the non-zero [C/O] ratio in metal-poor dwarf galaxies can have a strong impact on the characteristic stellar mass of IMF in a low-pressure but dense ISM. However, it does not have an appreciable impact on the IMF if the ISM is highly pressurized.

Measurements of the [C/O] ratio in galaxies with metallicities $7 < 12 + \log_{10} O/H < 7.7$ are highly desirable to constrain the transition of the IMF from top- to bottom-heavy.

5 CONCLUSIONS AND FUTURE OUTLOOK

There is compelling evidence for a non-solar scaling of the abundance of carbon with respect to oxygen in metal-poor environments. Specifically, observations find that the [C/O] ratio linearly changes with [O/H] at high metallicities, but flattens out at low [O/H], possibly also displaying an upturn below [O/H] = −3. At [O/H] < −1, the [C/O] ratio can vary by almost an order of magnitude (Amarsi et al. 2019c; Berg et al. 2019). While there has been immense work carried out to reproduce the observed [C/O]–[O/H] relation in metal-poor stars as well as metal-poor dwarf galaxies using IMF variations, the impact of the C and O abundances on the IMF has been largely unexplored.

In this work, we extend the calculations of collapsing dusty molecular clouds undergoing protostellar radiation feedback across a wide range of pressures, densities, and metallicities from primordial to supersolar (Sharda & Krumholz 2022). We particularly emphasize

the impacts of non-zero (or non-solar-scaled) [C/O] ratio on the characteristic stellar mass (or the peak mass, M_{ch}) of the IMF at low [O/H]. We find that as long as the ISM pressure is high, $P/k_B = 10^8$ K cm^{-3}, typical of superstar clusters and starburst galaxies, a non-constant [C/O] has no impact on M_{ch}, because dust completely dominates the thermodynamics of collapsing gas even at metallicities as low as [O/H] $= -3$, beyond which molecular H$_2$ takes over as the dominant gas coolant. A varying [C/O] ratio also does not seem to matter for the case where the ISM pressure is low, $P/k_B = 10^4$ K cm^{-3}, typical of main sequence star-forming galaxies, so long as the density is also low, or equivalently the cloud velocity dispersion is high.

Nonetheless, in the regime of pressure and gas density/velocity dispersion characteristic of giant molecular clouds in local galaxies, a varying [C/O] ratio significantly impacts M_{ch}. Using the observed trends in [C/O] as a function of [O/H] from two distinct sources – metal-poor stars in the Milky Way (Amarsi et al. 2019c) and metal-poor dwarf galaxies (Berg et al. 2019) – we show that the resulting M_{ch} implied by these trends can be different by a factor $\lesssim 7$ at $-3 \leq$ [O/H] ≤ -1. This is due to the reduction in the overall gas cooling rate due to low C abundances as compared to O. Additionally, the metallicity at which the IMF transitions from top- to bottom-heavy (i.e. where M_{ch} decreases from > 1 to $< 1\,M_\odot$) also shifts to higher [O/H] by ~ 1 dex. These results are rather insensitive to the choice of the chemical state of C and O in the ISM, or the adopted scaling of the dust-to-metal ratio with [O/H].

Thus, we find that the abundances of C and O significantly impact the IMF at low metallicities where cooling provided by fine structure metal lines dominates gas thermodynamics, at least in the case where the ISM pressure is low and density is high. Our results support the hypothesis that fine structure cooling by C and O lines plays a key role in the transition from Population III to II star formation (Bromm & Loeb 2003; Frebel et al. 2007). This finding also has potential consequences for the origin of CEMP-no stars; however, measurements of O abundance in these stars are needed. A characteristic IMF mass of $1{-}10\,M_\odot$ at $-2.5 \leq$ [O/H] ≤ -1.5 implies an overabundance of AGB stars that can re-enrich the metal-poor ISM with C on time-scales of the order of a few 100 Myr (Fishlock et al. 2014; Cristallo et al. 2015; Gil-Pons et al. 2022), potentially even driving [C/O] > 0 for the subsequent generation of star formation (e.g. CEMP-no stars). Note, however, that our models are restricted to predicting changes in the characteristic mass of the IMF, and not its entire functional form. It is possible that the slope at the high-mass end of the IMF is also impacted by a varying [C/O] ratio at low [O/H], an avenue we plan to investigate in future work.

Finding the IMF and the elemental abundances is an iterative process, since both impact each other in numerous ways. Given the new era of discoveries of very high-redshift galaxies by *JWST* with measurements of ISM abundances (e.g. Adams et al. 2022; Tacchella et al. 2022; Katz et al. 2023), it is now more important than ever to self-consistently model the IMF and the ISM abundances to correctly predict the yields of different elements (Krumholz et al. 2015), figure out dominant nucleosynthesis and feedback channels at low metallicities (Kobayashi et al. 2020), interpret metal distribution and ionization budget in the ISM (Sharda et al. 2021a), fit spectral energy distribution models to integrated galaxy spectra (Bellstedt et al. 2020), and more broadly, investigate star formation and metal enrichment in diverse, metal-poor environments.

ACKNOWLEDGEMENTS

DATA AVAILABILITY

The data we use in this work are available in Amarsi et al. (2019c) and Berg et al. (2019).

REFERENCES

Abate C., Pols O. R., Karakas A. I., Izzard R. G., 2015, A&A, 576, A118

Abdurro'uf et al., 2022, ApJS, 259, 35

Abohalima A., Frebel A., 2018, ApJS, 238, 36

Adams N. J. et al., 2022, MNRAS, Available at: https://doi.org/10.1093/mnras/stac3347

Akerman C. J., Carigi L., Nissen P. E., Pettini M., Asplund M., 2004, A&A, 414, 931

Akerman C. J., Ellison S. L., Pettini M., Steidel C. C., 2005, A&A, 440, 499

Amarsi A. M., Asplund M., Collet R., Leenaarts J., 2016, MNRAS, 455, 3735

Amarsi A. M., Barklem P. S., Asplund M., Collet R., Zatsarinny O., 2018, A&A, 616, A89

Amarsi A. M., Nissen P. E., Asplund M., Lind K., Barklem P. S., 2019a, A&A, 622, L4

Amarsi A. M., Barklem P. S., Collet R., Grevesse N., Asplund M., 2019b, A&A, 624, A111

Amarsi A. M., Nissen P. E., Skúladóttir Á., 2019c, A&A, 630, A104

Amorín R. et al., 2017, Nature Astron., 1, 0052

Aoki W., Beers T. C., Christlieb N., Norris J. E., Ryan S. G., Tsangarides S., 2007, ApJ, 655, 492

Aoki M., Aoki W., François P., 2020, A&A, 636, A111

Arellano-Córdova K. Z. et al., 2022, ApJ, 940, L23

Arentsen A., Starkenburg E., Shetrone M. D., Venn K. A., Depagne É., McConnachie A. W., 2019, A&A, 621, A108

Arentsen A. et al., 2020, MNRAS, 496, 4964

Arentsen A., Placco V. M., Lee Y. S., Aguado D. S., Martin N. F., Starkenburg E., Yoon J., 2022, MNRAS, 515, 4082

Asplund M., Grevesse N., Sauval A. J., Scott P., 2009, ARA&A, 47, 481

Bastian N., Saglia R. P., Goudfrooij P., Kissler-Patig M., Maraston C., Schweizer F., Zoccali M., 2006, A&A, 448, 881

Bastian N., Covey K. R., Meyer M. R., 2010, ARA&A, 48, 339

Bate M. R., 2014, MNRAS, 442, 285

Bate M. R., 2019, MNRAS, 484, 2341

Bate M. R., Keto E. R., 2015, MNRAS, 449, 2643

Bayliss M. B., Rigby J. R., Sharon K., Wuyts E., Florian M., Gladders M. D., Johnson T., Oguri M., 2014, ApJ, 790, 144

Beers T. C., Christlieb N., 2005, ARA&A, 43, 531

Bellstedt S. et al., 2020, MNRAS, 498, 5581

Berg D. A., Skillman E. D., Henry R. B. C., Erb D. K., Carigi L., 2016, ApJ, 827, 126

Berg D. A., Erb D. K., Auger M. W., Pettini M., Brammer G. B., 2018, ApJ, 859, 164

Berg D. A., Erb D. K., Henry R. B. C., Skillman E. D., McQuinn K. B. W., 2019, ApJ, 874, 93

Bessell M. S., Hughes S. M. G., Cottrell P. L., 1984, Publ. Astron. Soc. Aust., 5, 547

Bessell M. S., Sutherland R. S., Ruan K., 1991, ApJ, 383, L71

Bialy S., Sternberg A., 2015, MNRAS, 450, 4424

Boesgaard A. M., Rich J. A., Levesque E. M., Bowler B. P., 2011, ApJ, 743, 140

Bolatto A. D., Leroy A. K., Rosolowsky E., Walter F., Blitz L., 2008, ApJ, 686, 948

Bonifacio P. et al., 2015, A&A, 579, A28

Bonnor W. B., 1957, MNRAS, 117, 104

Bromm V., Loeb A., 2003, Nature, 425, 812

Bromm V., Ferrara A., Coppi P. S., Larson R. B., 2001, MNRAS, 328, 969

Buder S. et al., 2021, MNRAS, 506, 150

Byler N., Dalcanton J. J., Conroy C., Johnson B. D., Levesque E. M., Berg D. A., 2018, ApJ, 863, 14

Caffau E. et al., 2011, Nature, 477, 67

Cameron A. J. et al., 2021, ApJ, 918, L16

Carigi L., Hernandez X., 2008, MNRAS, 390, 582

Carigi L., Peimbert M., Esteban C., García-Rojas J., 2005, ApJ, 623, 213

Caselli P., Myers P. C., 1995, ApJ, 446, 665

Cazaux S., Spaans M., 2009, A&A, 496, 365

Chabrier G., 2003, PASP, 115, 763

Chabrier G., Hennebelle P., Charlot S., 2014, ApJ, 796, 75

Chakrabarti S., McKee C. F., 2005, ApJ, 631, 792

Chakrabarti S., Magnelli B., McKee C. F., Lutz D., Berta S., Popesso P., Pozzi F., 2013, ApJ, 773, 113

Chiaki G., Wise J. H., 2019, MNRAS, 482, 3933

Chiaki G., Yoshida N., 2022, MNRAS, 510, 5199

Chiaki G., Marassi S., Nozawa T., Yoshida N., Schneider R., Omukai K., Limongi M., Chieffi A., 2015, MNRAS, 446, 2659

Chiaki G., Yoshida N., Hirano S., 2016, MNRAS, 463, 2781

Chisholm J., Tremonti C., Leitherer C., 2018, MNRAS, 481, 1690

Chiti A. et al., 2018, ApJ, 856, 142

Chon S., Omukai K., Schneider R., 2021, MNRAS, 508, 4175

Chon S., Ono H., Omukai K., Schneider R., 2022, MNRAS, 514, 4639

Christensen L. et al., 2012, MNRAS, 427, 1973

Cohen M., Tielens A. G. G. M., Bregman J., Witteborn F. C., Rank D. M., Allamandola L. J., Wooden D., Jourdain de Muizon M., 1989, ApJ, 341, 246

Collet R., Asplund M., Trampedach R., 2006, ApJ, 644, L121

Collet R., Asplund M., Trampedach R., 2007, A&A, 469, 687

Collet R., Magic Z., Asplund M., 2011, J. Phys.: Conf. Ser., 328, 012003

Conroy C., van Dokkum P. G., 2012, ApJ, 760, 71

Cooke R. J., Pettini M., Jorgenson R. A., 2015, ApJ, 800, 12

Cooke R. J., Pettini M., Steidel C. C., 2017, MNRAS, 467, 802

Cristallo S., Straniero O., Piersanti L., Gobrecht D., 2015, ApJS, 219, 40

Dalcanton J. J., 2007, ApJ, 658, 941

Dame T. M., Hartmann D., Thaddeus P., 2001, ApJ, 547, 792

Draine B. T., 2011, Physics of the Interstellar and Intergalactic Medium. Princeton Univ. Press, Princeton, NJ

Ebert R., 1955, Z. Astrophys., 37, 217

Edmunds M. G., Pagel B. E. J., 1978, MNRAS, 185, 77P

Elmegreen B. G., Efremov Y. N., 1997, ApJ, 480, 235

Emerick A., Bryan G. L., Mac Low M.-M., Côté B., Johnston K. V., O'Shea B. W., 2018, ApJ, 869, 94

Erb D. K., Pettini M., Shapley A. E., Steidel C. C., Law D. R., Reddy N. A., 2010, ApJ, 719, 1168

Esteban C., Bresolin F., Peimbert M., García-Rojas J., Peimbert A., Mesa-Delgado A., 2009, ApJ, 700, 654

Esteban C., García-Rojas J., Carigi L., Peimbert M., Bresolin F., López-Sánchez A. R., Mesa-Delgado A., 2014, MNRAS, 443, 624

Ezzeddine R. et al., 2019, ApJ, 876, 97

Fabbian D., Nissen P. E., Asplund M., Pettini M., Akerman C., 2009, A&A, 500, 1143

Federrath C., Klessen R. S., 2013, ApJ, 763, 51

Filion C., Platais I., Wyse R. F. G., Kozhurina-Platais V., 2022, ApJ, 939, 38

Finn M. K., Johnson K. E., Brogan C. L., Wilson C. D., Indebetouw R., Harris W. E., Kamenetzky J., Bemis A., 2019, ApJ, 874, 120

Fishlock C. K., Karakas A. I., Lugaro M., Yong D., 2014, ApJ, 797, 44

Frebel A., Norris J. E., 2015, ARA&A, 53, 631

Frebel A., Johnson J. L., Bromm V., 2007, MNRAS, 380, L40

Frebel A., Collet R., Eriksson K., Christlieb N., Aoki W., 2008, ApJ, 684, 588

Frebel A., Simon J. D., Geha M., Willman B., 2010, ApJ, 708, 560

Frebel A., Norris J. E., Gilmore G., Wyse R. F. G., 2016, ApJ, 826, 110

Frebel A., Ji A. P., Ezzeddine R., Hansen T. T., Chiti A., Thompson I. B., Merle T., 2019, ApJ, 871, 146

Gallagher A. J., Caffau E., Bonifacio P., Ludwig H. G., Steffen M., Spite M., 2016, A&A, 593, A48

Gallagher A. J., Caffau E., Bonifacio P., Ludwig H. G., Steffen M., Homeier D., Plez B., 2017, A&A, 598, L10

Galli D., Palla F., 1998, A&A, 335, 403

García Pérez A. E., Asplund M., Primas F., Nissen P. E., Gustafsson B., 2006, A&A, 451, 621

García-Rojas J., Esteban C., 2007, ApJ, 670, 457

Garnett D. R., Skillman E. D., Dufour R. J., Peimbert M., Torres-Peimbert S., Terlevich R., Terlevich E., Shields G. A., 1995, ApJ, 443, 64

Garnett D. R., Shields G. A., Peimbert M., Torres-Peimbert S., Skillman E. D., Dufour R. J., Terlevich E., Terlevich R. J., 1999, ApJ, 513, 168

Gennaro M. et al., 2018, ApJ, 855, 20

Gieser C. et al., 2021, A&A, 648, A66

Gil-Pons P., Doherty C. L., Campbell S. W., Gutiérrez J., 2022, A&A, preprint (arXiv:2209.05587)

Glover S. C. O., Clark P. C., 2012, MNRAS, 426, 377

Glover S. C. O., Clark P. C., 2016, MNRAS, 456, 3596

González Hernández J. I., Bonifacio P., Ludwig H. G., Caffau E., Behara N. T., Freytag B., 2010, A&A, 519, A46

Grasha K., Roy A., Sutherland R. S., Kewley L. J., 2021, ApJ, 908, 241

Grasha K. et al., 2022, ApJ, 929, 118

Grevesse N., Asplund M., Sauval A. J., Scott P., 2010, Ap&SS, 328, 179

Gu M., Greene J. E., Newman A. B., Kreisch C., Quenneville M. E., Ma C.-P., Blakeslee J. P., 2022, ApJ, 932, 103

Guadarrama R., Vorobyov E. I., Rab C., Güdel M., 2022, A&A, 667, A28

Gustafsson B., Karlsson T., Olsson E., Edvardsson B., Ryde N., 1999, A&A, 342, 426

Guszejnov D., Krumholz M. R., Hopkins P. F., 2016, MNRAS, 458, 673

Hansen T. T., Andersen J., Nordström B., Beers T. C., Placco V. M., Yoon J., Buchhave L. A., 2016, A&A, 586, A160

Harris C. R. et al., 2020, Nature, 585, 357

Hayes C. R. et al., 2022, ApJS, 262, 34

Henry R. B. C., Edmunds M. G., Köppen J., 2000, ApJ, 541, 660

Hopkins A. M., 2018, Publ. Astron. Soc. Aust., 35, e039

Hou K.-C., Aoyama S., Hirashita H., Nagamine K., Shimizu I., 2019, MNRAS, 485, 1727

Hu C.-Y., Sternberg A., van Dishoeck E. F., 2021, ApJ, 920, 44

Hunter J. D., 2007, Comput. Sci. Eng., 9, 90

Ishigaki M. N., Aoki W., Arimoto N., Okamoto S., 2014, A&A, 562, A146

Israelian G., Ecuvillon A., Rebolo R., García-López R., Bonifacio P., Molaro P., 2004, A&A, 421, 649

Iwamoto N., Umeda H., Tominaga N., Nomoto K., Maeda K., 2005, Science, 309, 451

James B. L. et al., 2014, MNRAS, 440, 1794

Jameson K. E. et al., 2018, ApJ, 853, 111

Jenkins E. B., 2014, preprint (arXiv:1402.4765)

Ji A. P., Frebel A., Simon J. D., Geha M., 2016, ApJ, 817, 41

Johnson J. L., 2015, MNRAS, 453, 2771

Johnson K. E., Leroy A. K., Indebetouw R., Brogan C. L., Whitmore B. C., Hibbard J., Sheth K., Evans A. S., 2015, ApJ, 806, 35

Johnson J. W., Weinberg D. H., Vincenzo F., Bird J. C., Griffith E. J., 2022, MNRAS, preprint (arXiv:2202.04666)

Katz H. et al., 2023, MNRAS, 518, 592

Kepley A. A., Leroy A. K., Johnson K. E., Sandstrom K., Chen C. H. R., 2016, ApJ, 828, 50

Kewley L. J., Nicholls D. C., Sutherland R., Rigby J. R., Acharya A., Dopita M. A., Bayliss M. B., 2019, ApJ, 880, 16

Kobayashi C., Karakas A. I., Lugaro M., 2020, ApJ, 900, 179

Kobulnicky H. A., Skillman E. D., 1996, ApJ, 471, 211

Komiya Y., Suda T., Minaguchi H., Shigeyama T., Aoki W., Fujimoto M. Y., 2007, ApJ, 658, 367

Konstantopoulou C. et al., 2022, A&A, 666, A12

Kroupa P., 2001, MNRAS, 322, 231

Krumholz M. R., 2011, ApJ, 743, 110

Krumholz M. R., 2014, MNRAS, 437, 1662

Krumholz M. R., McKee C. F., Tumlinson J., 2009, ApJ, 693, 216

Krumholz M. R., Klein R. I., McKee C. F., 2011, ApJ, 740, 74

Krumholz M. R., Fumagalli M., da Silva R. L., Rendahl T., Parra J., 2015, MNRAS, 452, 1447

Krumholz M. R., Myers A. T., Klein R. I., McKee C. F., 2016, MNRAS, 460, 3272

Lacchin E., Matteucci F., Vincenzo F., Palla M., 2020, MNRAS, 495, 3276

Langer W. D., 2009, in Lis D. C., Vaillancourt J. E., Goldsmith P. F., Bell T. A., Scoville N. Z., Zmuidzinas J., eds, ASP Conf. Ser. Vol. 417, Submillimeter Astrophysics and Technology: A Symposium Honoring Thomas G. Phillips. Astron. Soc. Pac., San Francisco, p. 71

Li Q., Narayanan D., Davé R., 2019, MNRAS, 490, 1425

Liang Y. C., Yin S. Y., Hammer F., Deng L. C., Flores H., Zhang B., 2006, ApJ, 652, 257

Llerena M. et al., 2022, A&A, 659, A16

López-Sánchez Á. R., Esteban C., García-Rojas J., Peimbert M., Rodríguez M., 2007, ApJ, 656, 168

Lopez L. A., Mathur S., Nguyen D. D., Thompson T. A., Olivier G. M., 2020, ApJ, 904, 152

Lucey M. et al., 2022, MNRAS, preprint (arXiv:2206.08299)

Mac Low M.-M., Ferrara A., 1999, ApJ, 513, 142

McKee C. F., Krumholz M. R., 2010, ApJ, 709, 308

Madden S. C. et al., 2020, A&A, 643, A141

Maeder A., 1992, A&A, 264, 105

Magic Z., Collet R., Asplund M., Trampedach R., Hayek W., Chiavassa A., Stein R. F., Nordlund A., 2013, A&A, 557, A26

Mardini M. K. et al., 2022, MNRAS, 517, 3993

Martín-Navarro I. et al., 2015, ApJ, 806, L31

Mathis J. S., 1990, ARA&A, 28, 37

Mattsson L., 2010, A&A, 515, A68

Meece G. R., Smith B. D., O'Shea B. W., 2014, ApJ, 783, 75

Mingozzi M. et al., 2022, ApJ, 939, 110

Miville-Deschênes M.-A., Murray N., Lee E. J., 2017, ApJ, 834, 57

Munshi F., Christensen C., Quinn T. R., Governato F., Wadsley J., Loebman S., Shen S., 2014, ApJ, 781, L14

Myers A. T., Krumholz M. R., Klein R. I., McKee C. F., 2011, ApJ, 735, 49

Nagasawa D. Q. et al., 2018, ApJ, 852, 99

Nicholls D. C., Sutherland R. S., Dopita M. A., Kewley L. J., Groves B. A., 2017, MNRAS, 466, 4403

Nissen P. E., Gustafsson B., 2018, A&AR, 26, 6

Nissen P. E., Akerman C., Asplund M., Fabbian D., Kerber F., Kaufl H. U., Pettini M., 2007, A&A, 469, 319

Nissen P. E., Chen Y. Q., Carigi L., Schuster W. J., Zhao G., 2014, A&A, 568, A25

Nordlander T. et al., 2019, MNRAS, 488, L109

Norris J. E., Yong D., 2019, ApJ, 879, 37

Norris J. E. et al., 2013, ApJ, 762, 28

Oliphant T. E., 2006, A Guide to NumPy. Vol. 1. Trelgol Publishing, USA

Omukai K., 2000, ApJ, 534, 809

Omukai K., 2012, PASJ, 64, 114

Omukai K., Tsuribe T., Schneider R., Ferrara A., 2005, ApJ, 626, 627

Omukai K., Hosokawa T., Yoshida N., 2010, ApJ, 722, 1793

Padoan P., Nordlund A., Jones B. J. T., 1997, MNRAS, 288, 145

Palla M., Calura F., Matteucci F., Fan X. L., Vincenzo F., Lacchin E., 2020, MNRAS, 494, 2355

Papadopoulos P. P., 2010, ApJ, 720, 226

Peimbert A., Peimbert M., 2010, ApJ, 724, 791

Pérez-Montero E., Contini T., 2009, MNRAS, 398, 949

Pilyugin L. S., Thuan T. X., 2005, ApJ, 631, 231

Pineda J. L. et al., 2017, ApJ, 839, 107

Popping G., Péroux C., 2022, MNRAS, 513, 1531

Popping G., Somerville R. S., Galametz M., 2017, MNRAS, 471, 3152

Rémy-Ruyer A. et al., 2014, A&A, 563, A31

Rigby J. R. et al., 2018, ApJ, 853, 87

Robles-Valdez F., Rodríguez-González A., Hernández-Martínez L., Esquivel A., 2017, ApJ, 835, 136

Romano D., 2022, A&AR, 30, 7

Romano D., Matteucci F., Zhang Z.-Y., Ivison R. J., Ventura P., 2019a, MNRAS, 490, 2838

Romano D., Calura F., D'Ercole A., Few C. G., 2019b, A&A, 630, A140

Romano D., Franchini M., Grisoni V., Spitoni E., Matteucci F., Morossi C., 2020, A&A, 639, A37

Rossi M., Salvadori S., Skúladóttir Á., 2021, MNRAS, 503, 6026

Roy A., Dopita M. A., Krumholz M. R., Kewley L. J., Sutherland R. S., Heger A., 2021, MNRAS, 502, 4359

Rubio M., Elmegreen B. G., Hunter D. A., Brinks E., Cortés J. R., Cigan P., 2015, Nature, 525, 218

Salvadori S., Ferrara A., 2012, MNRAS, 421, L29

Schneider R., Omukai K., 2010, MNRAS, 402, 429

Schneider R., Omukai K., Inoue A. K., Ferrara A., 2006, MNRAS, 369, 1437

Schneider R., Omukai K., Bianchi S., Valiante R., 2012, MNRAS, 419, 1566

Schneider N. et al., 2015, A&A, 578, A29

Schöier F. L., van der Tak F. F. S., van Dishoeck E. F., Black J. H., 2005, A&A, 432, 369

Schruba A. et al., 2017, ApJ, 835, 278

Sharda P., Krumholz M. R., 2022, MNRAS, 509, 1959

Sharda P., Krumholz M. R., Federrath C., 2019, MNRAS, 490, 513

Sharda P., Krumholz M. R., Wisnioski E., Forbes J. C., Federrath C., Acharyya A., 2021a, MNRAS, 502, 5935

Sharda P., Federrath C., Krumholz M. R., Schleicher D. R. G., 2021b, MNRAS, 503, 2014

Sharda P., Krumholz M. R., Wisnioski E., Acharyya A., Federrath C., Forbes J. C., 2021c, MNRAS, 504, 53

Sharda P. et al., 2022, MNRAS, 509, 2180

Sharma M., Theuns T., Frenk C. S., Cooke R. J., 2018, MNRAS, 473, 984

Shi Y., Wang J., Zhang Z.-Y., Gao Y., Hao C.-N., Xia X.-Y., Gu Q., 2016, Nature Commun., 7, 13789

Shima K., Hosokawa T., 2021, MNRAS, 508, 4767

Skúladóttir Á. et al., 2021, ApJ, 915, L30

Smith R. J., 2020, ARA&A, 58, 577

Sofia U. J., Parvathi V. S., Babu B. R. S., Murthy J., 2011, AJ, 141, 22

Spite M. et al., 2005, A&A, 430, 655

Stark D. P. et al., 2014, MNRAS, 445, 3200

Stasińska G., 1978, A&A, 66, 257

Steidel C. C., Strom A. L., Pettini M., Rudie G. C., Reddy N. A., Trainor R. F., 2016, ApJ, 826, 159

Sternberg A., Le Petit F., Roueff E., Le Bourlot J., 2014, ApJ, 790, 10

Sternberg A., Gurman A., Bialy S., 2021, ApJ, 920, 83

Suda T., Yamada S., Katsuta Y., Komiya Y., Ishizuka C., Aoki W., Fujimoto M. Y., 2011, MNRAS, 412, 843

Suda T. et al., 2013, MNRAS, 432, L46

Tacchella S. et al., 2022, preprint (arXiv:2208.03281)

Tanvir T. S., Krumholz M. R., Federrath C., 2022, MNRAS, 516, 5712

Toribio San Cipriano L., Domínguez-Guzmán G., Esteban C., García-Rojas J., Mesa-Delgado A., Bresolin F., Rodríguez M., Simón-Díaz S., 2017, MNRAS, 467, 3759

Triani D. P., Sinha M., Croton D. J., Pacifici C., Dwek E., 2020, MNRAS, 493, 2490

Tsujimoto T., Bekki K., 2011, A&A, 530, A78

Turner J. L., Beck S. C., Ho P. T. P., 2000, ApJ, 532, L109

van der Tak F. F. S., van Dishoeck E. F., Evans Neal J. I., Blake G. A., 2000, ApJ, 537, 283

van der Tak F. F. S., Black J. H., Schöier F. L., Jansen D. J., van Dishoeck E. F., 2007, A&A, 468, 627

van der Tak F. F. S., Lique F., Faure A., Black J. H., van Dishoeck E. F., 2020, Atoms, 8, 15

van Dokkum P. G., Conroy C., 2010, Nature, 468, 940

van Dokkum P. G. et al., 2008, ApJ, 677, L5

van Zee L., Haynes M. P., 2006, ApJ, 636, 214

Vanzella E. et al., 2016, ApJ, 821, L27

Vijayan A. P., Clay S. J., Thomas P. A., Yates R. M., Wilkins S. M., Henriques B. M., 2019, MNRAS, 489, 4072

Virtanen P. et al., 2020, Nature Methods, 17, 261

Welty D. E., Lauroesch J. T., Wong T., York D. G., 2016, ApJ, 821, 118

Yamaguchi N., Furlanetto S. R., Trapp A. C., 2022, MNRAS, preprint (arXiv: 2209.09345)

Yin J., Matteucci F., Vladilo G., 2011, A&A, 531, A136

Yong D. et al., 2021, MNRAS, 507, 4102

Yoon J. et al., 2016, ApJ, 833, 20

Yoon J., Beers T. C., Tian D., Whitten D. D., 2019, ApJ, 878, 97

Youakim K. et al., 2020, MNRAS, 492, 4986

Zepeda J. et al., 2022, preprint (arXiv:2209.12224)

Zubko V., Dwek E., Arendt R. G., 2004, ApJS, 152, 211

This paper has been typeset from a TeX/LaTeX file prepared by the author.